

Figure 1. Reference map of the Fucino Basin. (a) Location of Fucino Basin with respect to the main Quaternary Italian volcanic centres. (b) Shaded relief map showing the location of the GL, TS, SP, F1-F3 (Giaccio et al., 2015b; 2017a), F4-F5 (Mannella et al., 2019, this study), FUC-S5-6 (Di Roberto et al., 2018) boreholes in the Fucino Basin. See legend in inset for the meaning of symbols. (c) Seismic Line 1 (see trace in panel b) showing the internal architecture of the Plio-Quaternary continental deposits of the Fucino Basin along a W-E oriented profile (Cavinato et al., 2002). The projected location of various boreholes on Line 1 is also shown. Seismic facies interpretation of the sedimentary infill is according to Cavinato et al. (2002).

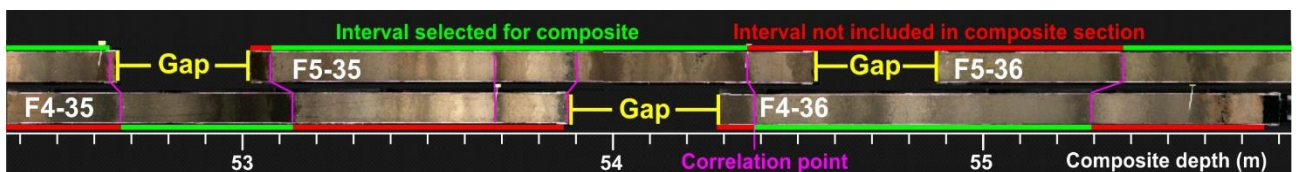


Figure 2. Example of correlation between the overlapped F4 and F5 core sections and of the selection of the intervals used for building the composite F4-F5 record. Note that the gaps in-between two consecutive individual core sections of F4 borehole are documented in F5 borehole, and vice versa.

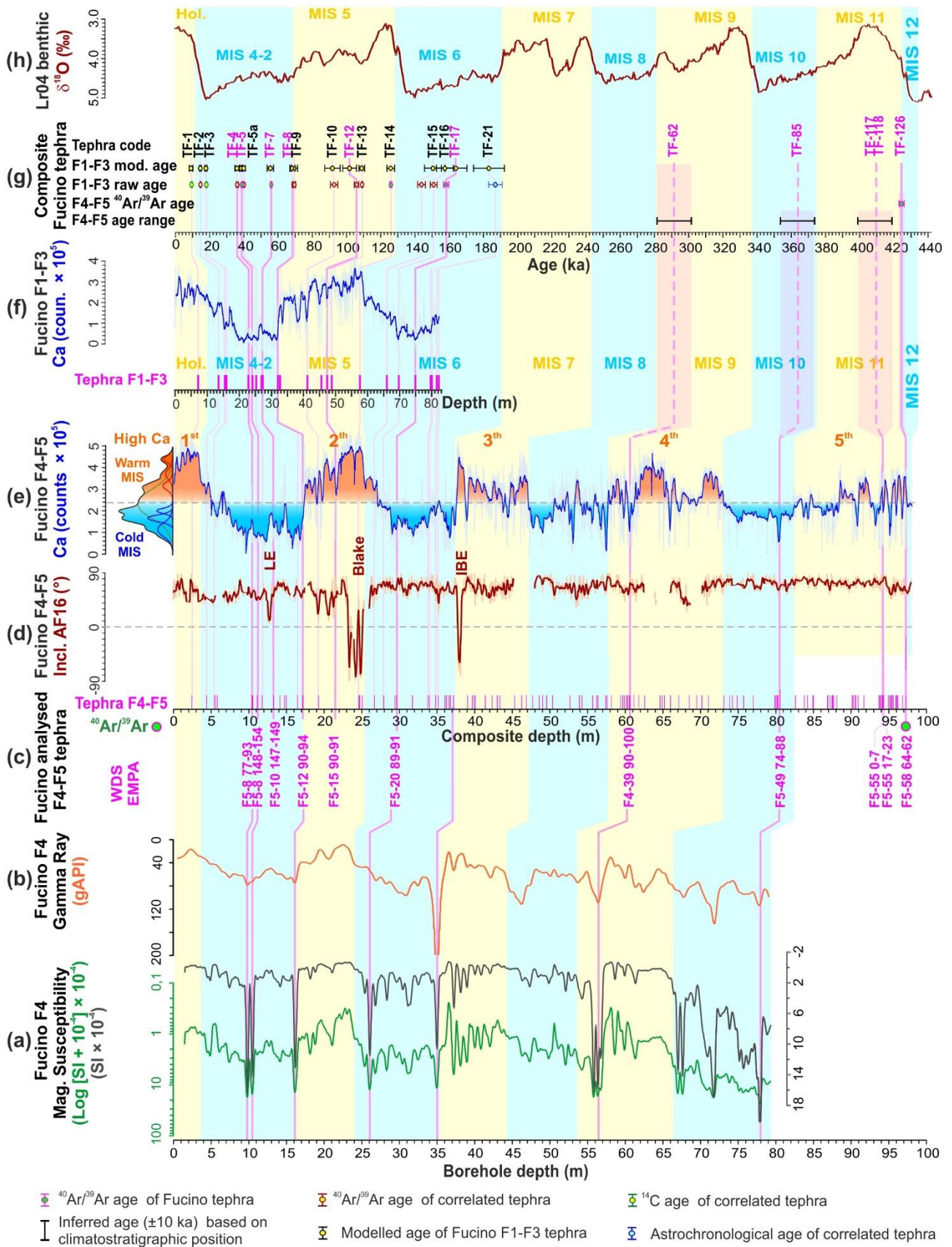


Figure 3. Tephrostratigraphy, selected proxy data and general chronological framework for the newly F4-F5 and the previously investigated F1-F3 (Giaccio et al., 2017; Mannella et al., 2019). (a) Magnetic susceptibility from Fucino F4 downhole logging (black) and its logarithmic representation (green) to show similarity to gamma ray and Ca data. (b) Gamma ray from Fucino F4 downhole logging. (c) Selected tephra from core F4-

F5 investigated in this study. **(d)** Inclination data after the 16 mT AF step with tentative position of the Laschamp (LE) Blake and Iceland Basin (IBE) geomagnetic excursions. **(e)** Complete tephra record and Ca counts from XRF scanning in core F4-F5. Five stratigraphic intervals with relatively high Ca counts are highlighted in yellow and correlated to the warm Marine Isotope Stage (MIS) 1 to 11 (the threshold is at 22700 cps, see text for explanation). **(f)** Complete tephra record and Ca counts from XRF scanning in core F1-F3 (Giaccio et al., 2017; Mannella et al., 2019). **(g)** Combined tephrochronology of F1-F3 and F4-F5 core. **(h)** LR04 stack of marine benthic oxygen isotope records (Lisiecki and Raymo, 2005). Data source: $^{40}\text{Ar}/^{39}\text{Ar}$, ^{14}C , astrochronological, modelled ages and correlation of tephra of the last 190 kyr: Giaccio et al. (2017) and Mannella et al. (2019) and reference therein. The boundaries of the marine isotope stages (MIS) are according to Railsback et al. (2015).

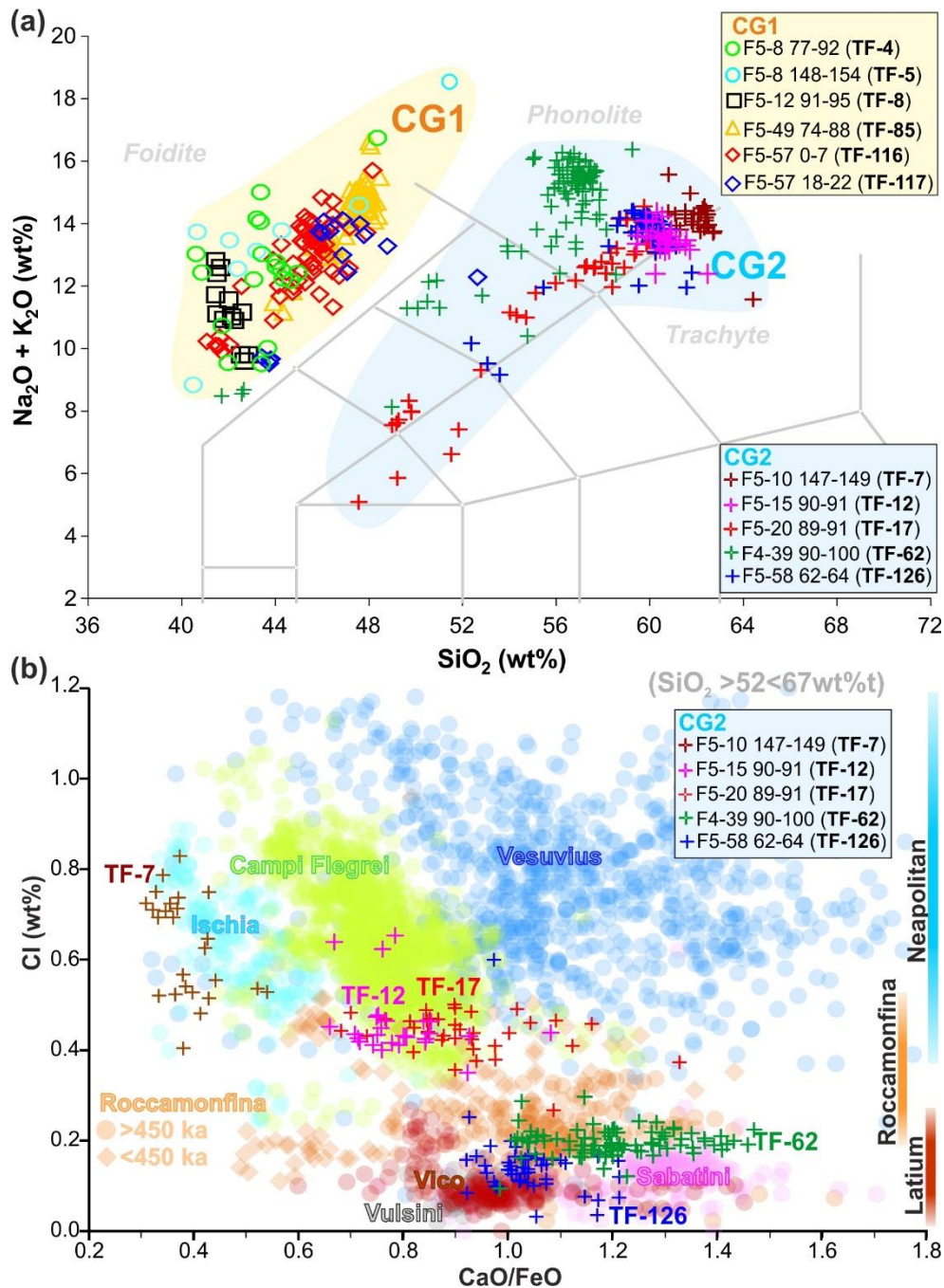


Figure 4. Representative major element compositions for the analysed F4-F5 tephra layers. **(a)** Total alkali versus silica classification diagram (Le Bas et al., 1986) of the F4-F5 tephra distinguished in two compositional groups (CG1 and CG2). **(b)** CaO/FeO vs Cl discriminating diagram of the volcanic sources of the Italian

potassic trachyte-phonolite and tephriphonolite tephra (modified from Giaccio et al., 2017) for the F4-F5 tephra. The CaO/FeO vs Cl diagram has been updated with the following data: Roccamonfina: Amato et al. (2014) and Galli et al. (2017); Vulcini, Vico Period I (P-I) and Period II (P-II) and Sabatini: this study and Author's unpublished data. For other references, the readers are referred to Giaccio et al. (2017).

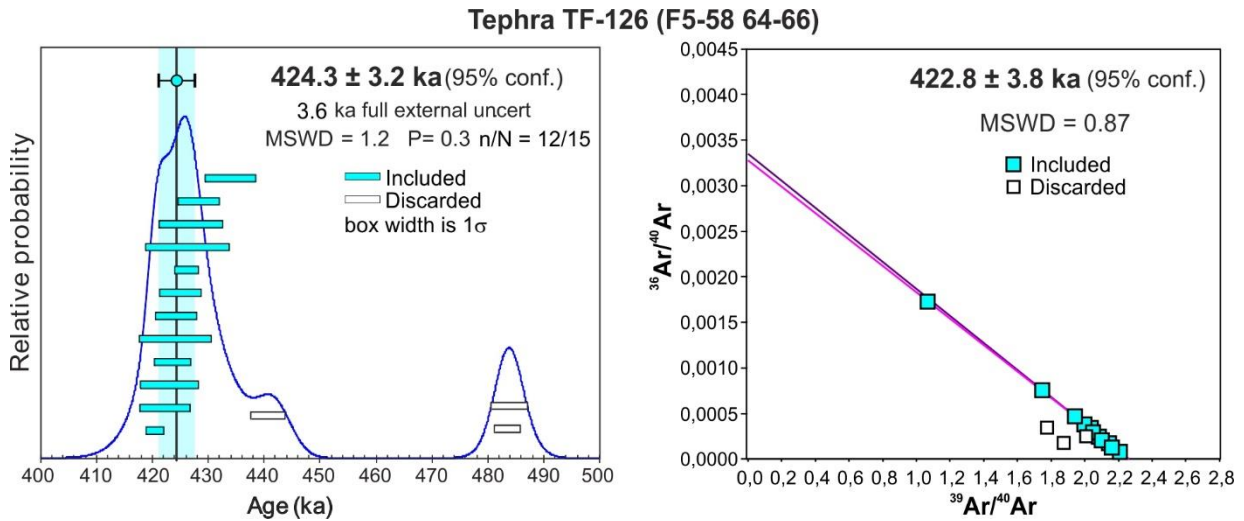
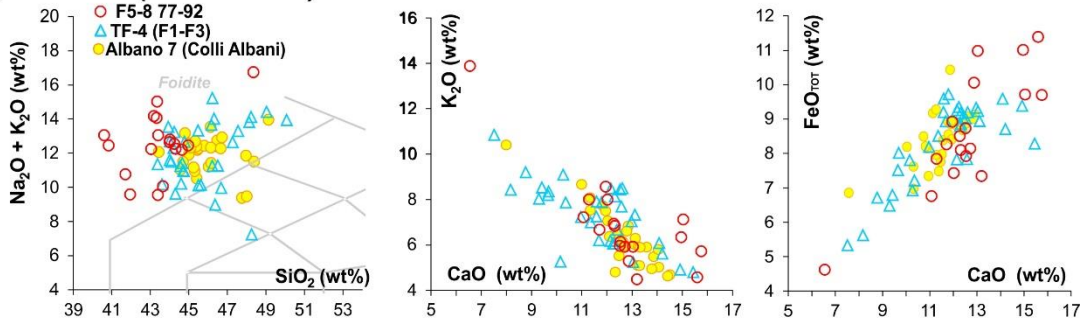
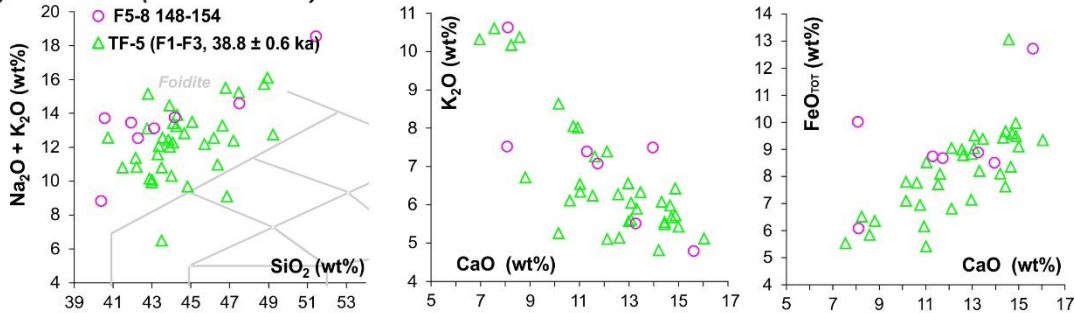


Figure 5. Age probability density spectra diagram (left) and inverse isochrone (right) of tephra TF-126 (sampling code; F5-58 64-66). Blue and white bars/ indicate the individual ages included and discarded as weighted mean age, respectively.

(a) Albano 7 (35.8 ± 1.2 ka)



(b) Albano 5 (38.8 ± 1.4 ka)



(c) Albano 3 (70.0 ± 2.0 ka)

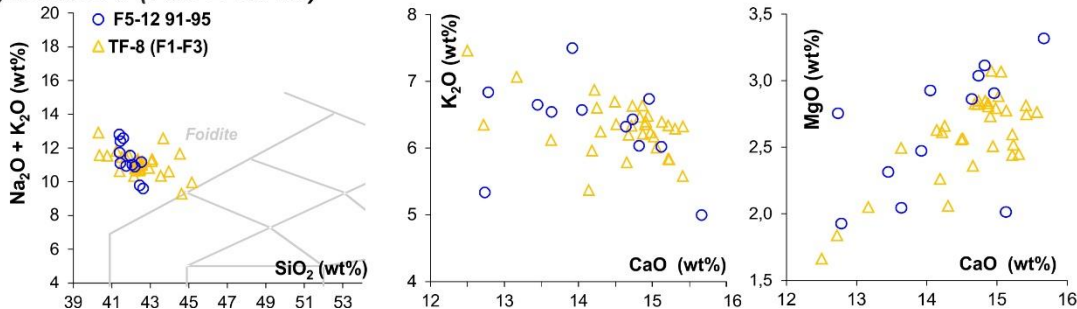
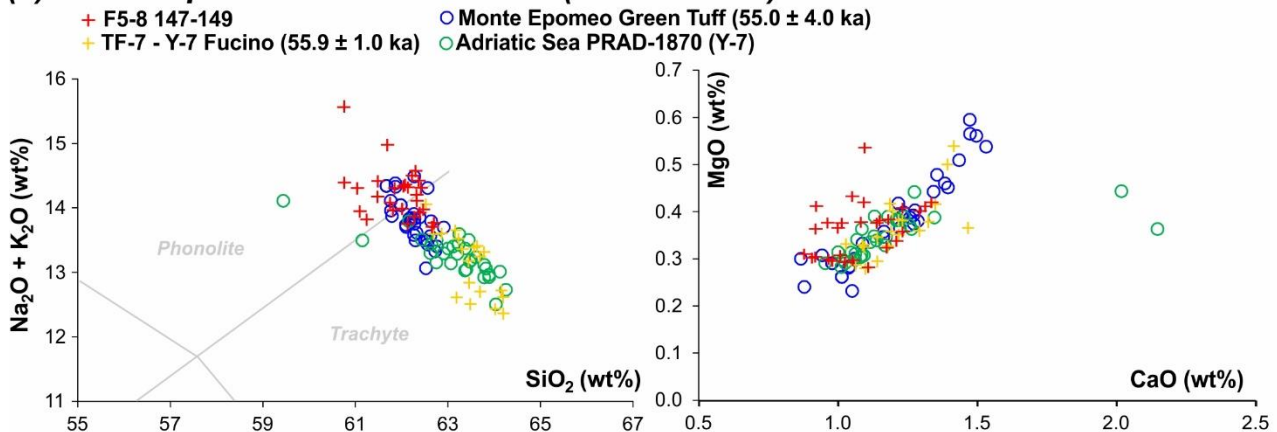
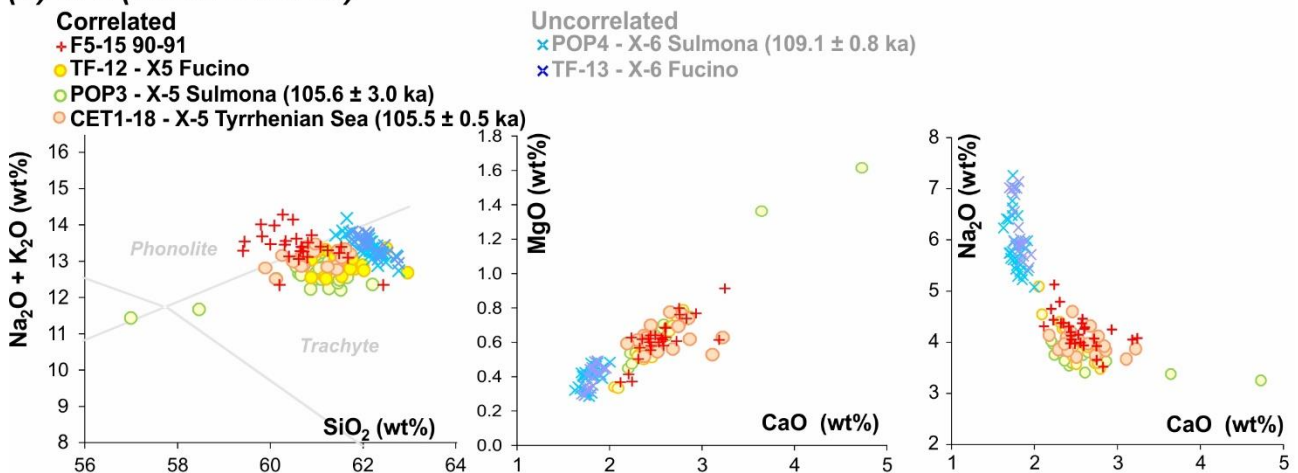


Figure 6. Total alkali versus silica classification diagram after Le Bas et al. (1986) and representative bi-plots for the tephra F5-8 77-92 (a), F5-8 148-155 (b) and F8-12 89-91 (c) from the F4-F5 record compared with their equivalents in core F1-F3. Data source: glass-WDS of Fucino TF-4, TF-5 and TF-8: Giaccio et al. (2017); $^{40}\text{Ar}/^{39}\text{Ar}$ age of Fucino TF-5: weighted mean of dating from (Freda et al., 2006; Giaccio et al., 2009; Giaccio et al., 2017), and Mannella et al. (2019); glass composition of Albano 7 Colli Albani: Giaccio et al. (2007); $^{40}\text{Ar}/^{39}\text{Ar}$ age of Albano 7 and Albano 3: weighted mean of dating from Freda et al. (2006) and Giaccio et al. (2007). $^{40}\text{Ar}/^{39}\text{Ar}$ ages are recalculated relative to an age of 1.1891 Ma for the Alder Creek sanidine monitor standard (Niespolo et al., 2017), with the uncertainty expressed at 2σ .

(a) Monte Epomeo Green Tuff - Y-7 (55.9 ± 1.0 ka)



(b) X-5 (105.6 ± 0.5 ka)



(c) Taurano Ignimbrite (159.4 ± 1.6 ka)

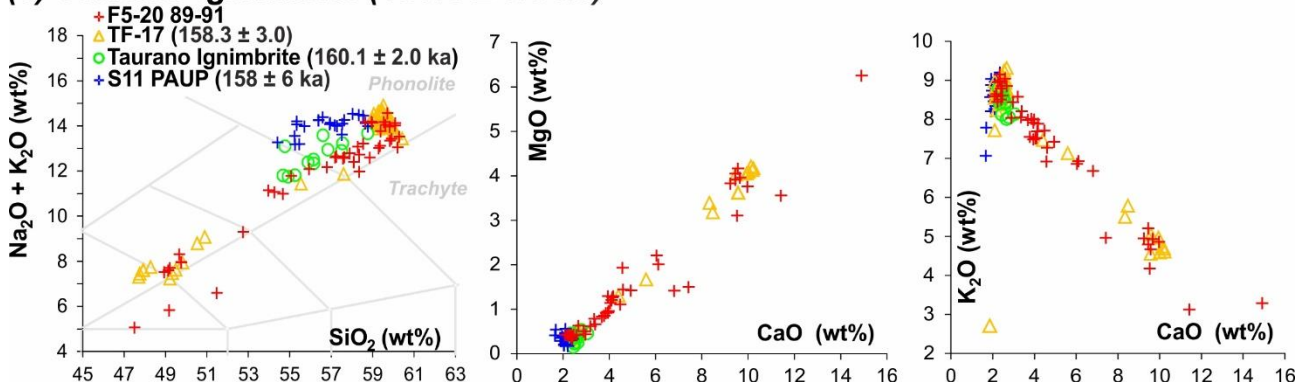
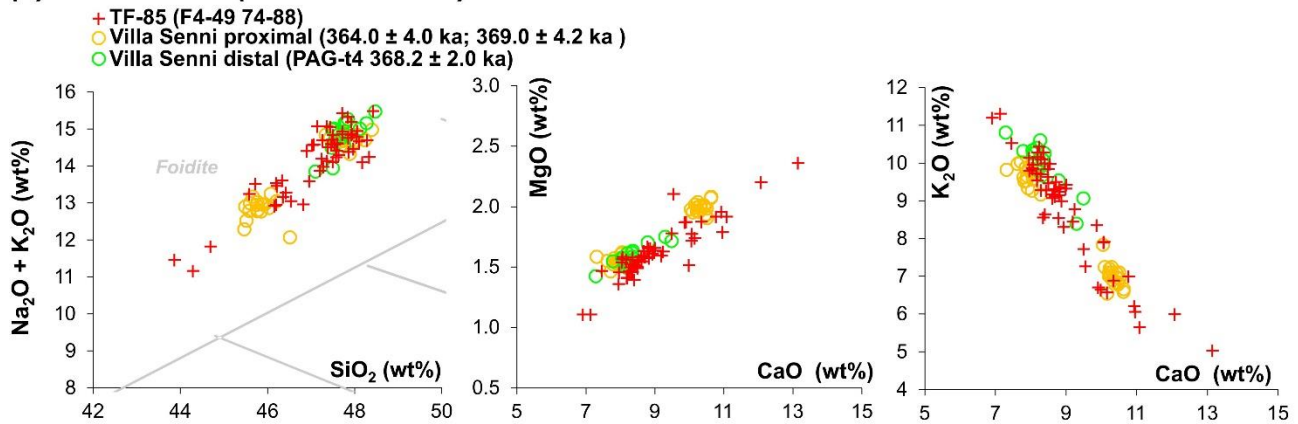


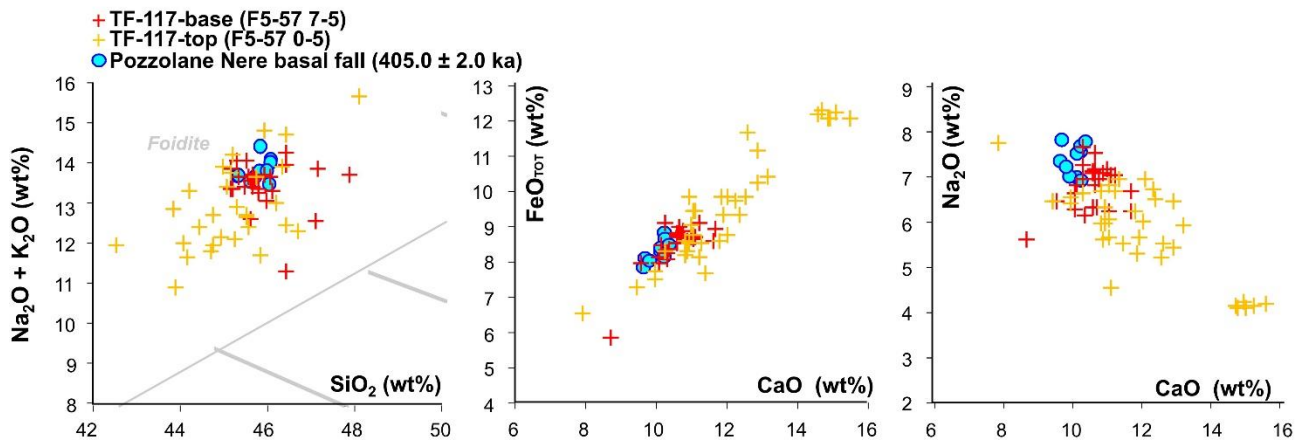
Figure 7. Total alkali versus silica classification diagram Le Bas et al. (1986) and representative bi-plots for the tephra F5-8 148-149 (a), F5-15 90-91 (b), F5-20 89-91 (c) from core F4-F5 compared with their equivalents in core F1-F3 and with some selected proximal or distal counterparts. For comparison, in panel (b) also the composition of X-6 layer (grey text), not correlated with F5-15 90-91, is shown. Data source: glass-WDS and

$^{40}\text{Ar}/^{39}\text{Ar}$ age of Fucino TF-7: Giaccio et al. (2017); glass-WDS and $^{40}\text{Ar}/^{39}\text{Ar}$ age of Monte Epomeo Green Tuff: Tomlinson et al. (2014)) and Sbrana and Toccaceli (2011), respectively; glass-WDS of PRAD-1870: Bourne et al. (2010); glass-WDS TF-12 and TF-13 Giaccio et al. (2017); glass-WDS and $^{40}\text{Ar}/^{39}\text{Ar}$ age of Sulmona POP3 and POP4 tephra layers: Giaccio et al. (2012b) and Regattieri et al. (2015), respectively; glass-EDS glass-WDS and $^{40}\text{Ar}/^{39}\text{Ar}$ age of TF-17: Giaccio et al. (2017); glass-EDS and $^{40}\text{Ar}/^{39}\text{Ar}$ age of CET1-18: Petrosino et al. (2016); glass-EDS and $^{40}\text{Ar}/^{39}\text{Ar}$ age of the proximal Taurano Ignimbrite: Amato et al. (2018) and De Vivo et al. (2001), respectively; glass-EDS and $^{40}\text{Ar}/^{39}\text{Ar}$ age of S11 PAUP: Amato et al. (2018). The tephra age reported on top of each figure panel is the weighted mean of the $^{40}\text{Ar}/^{39}\text{Ar}$ ages indicated in the respective panel. $^{40}\text{Ar}/^{39}\text{Ar}$ ages are recalculated relatively to an age of 1.1891 Ma for the Alder Creek sanidine monitor standard (Niespolo et al., 2017), with the uncertainty expressed at 2σ .

(a) Villa Senni (367.5 ± 1.6 ka)



(b) Pozzolane Nere (405.0 ± 2.0 ka)



(c) Pozzolane Nere precursor (407.1 ± 4.2 ka)

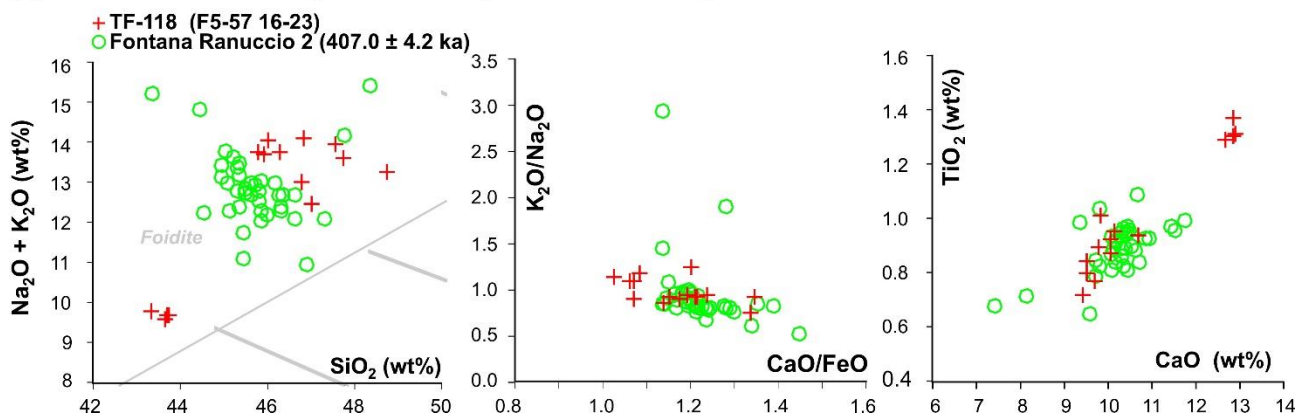
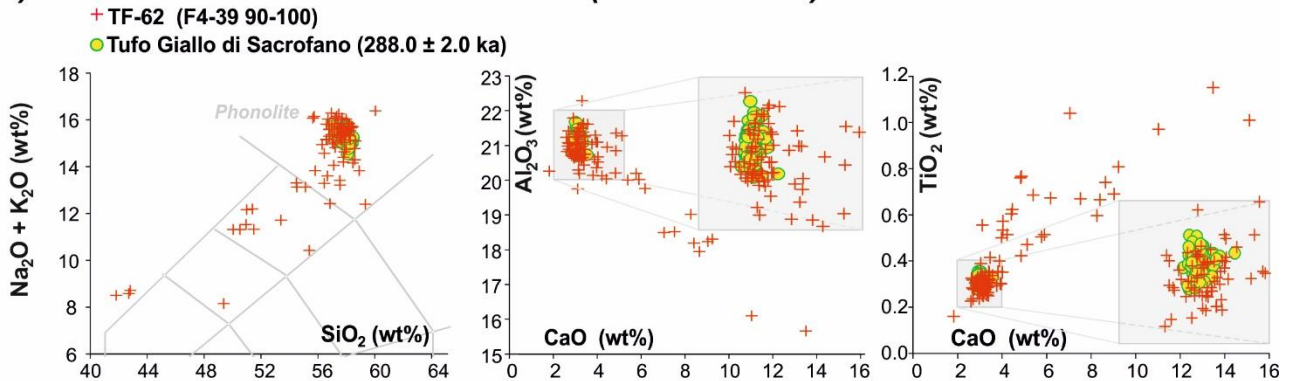


Figure 8. Total alkali versus silica classification diagram after Le Bas et al. (1986) and representative bi-plots for the tephra TF-85 (a), TF-117 (b), and TF-118 (c) from the F4-F5 record compared with their proximal or distal counterparts. Data source: glass-WDS and $^{40}\text{Ar}/^{39}\text{Ar}$ age of Villa Senni proximal units: (Marra et al., 2009, 2019); glass-WDS and $^{40}\text{Ar}/^{39}\text{Ar}$ age of Villa Senni distal (PAG-t4): (Giaccio et al., 2012a); glass-WDS and $^{40}\text{Ar}/^{39}\text{Ar}$ age Pozzolane Nere fallout: (glass-WDS): (Marra et al., 2009); glass-WDS and $^{40}\text{Ar}/^{39}\text{Ar}$ age Fontana Ranuccio 2 (glass-WDS): (Pereira et al., 2018). The tephra age reported on top of each figure panel is the weighted mean of the $^{40}\text{Ar}/^{39}\text{Ar}$ ages indicated in the respective panel. $^{40}\text{Ar}/^{39}\text{Ar}$ ages are recalculated

(a) Sabatini - Tufo Giallo di Sacrofano (288.0 ± 2.0 ka)



(b) Vulsini - Castel Broco (424.3 ± 3.2 ka)

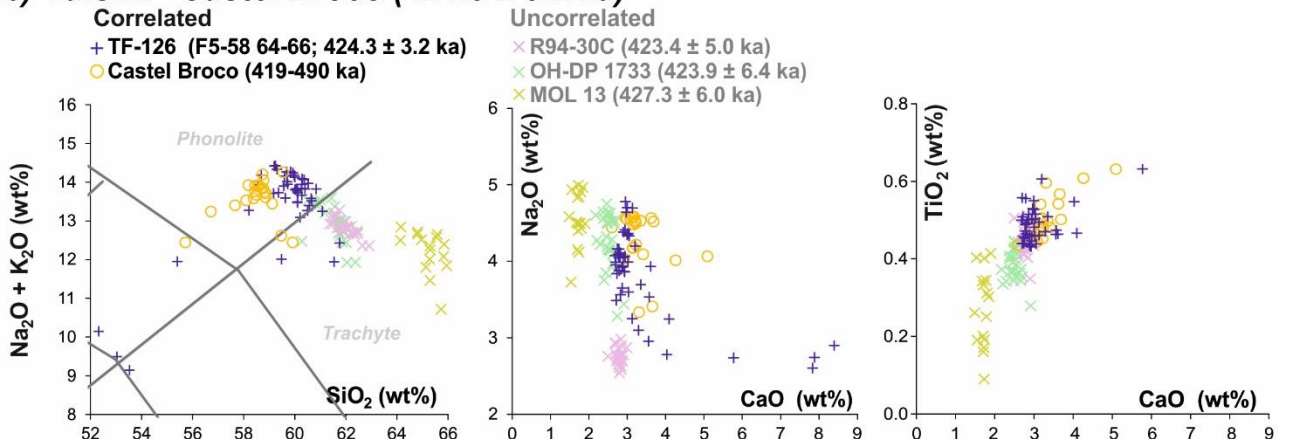


Figure 9. Total alkali versus silica classification diagram after Le Bas et al. (1986) and representative bi-plots for the tephra TF-62 (a) and TF-126 (b) of the F4-F5 succession compared with their proximal counterparts. TF-126 is also compared with some geochronologically compatible but geochemically different tephra R99-30C (Tiber River successions), OH-DP 1733 (Lake Ohrid) and MOL 13 (Bojano Basin). Data source: glass-WDS of Tufo Giallo di Sacrofano and Castel Broco: this study; $^{40}\text{Ar}/^{39}\text{Ar}$ age of Tufo Giallo di Sacrofano: Sottili et al. (2010); glass-WDS and $^{40}\text{Ar}/^{39}\text{Ar}$ age of R94-30C: this study and Marra et al. (2016) respectively; glass-WDS of OH-DP 1733: Leicher et al. (in review); glass-WDS of MOL 13: Amato et al. (2014). The tephra age reported on top of each figure panel is the weighted mean of the $^{40}\text{Ar}/^{39}\text{Ar}$ ages indicated in the respective panel. $^{40}\text{Ar}/^{39}\text{Ar}$ ages are recalculated relatively to an age of 1.1891 Ma for the Alder Creek sanidine monitor standard (Niespolo et al., 2017), with the uncertainty expressed at 2σ .

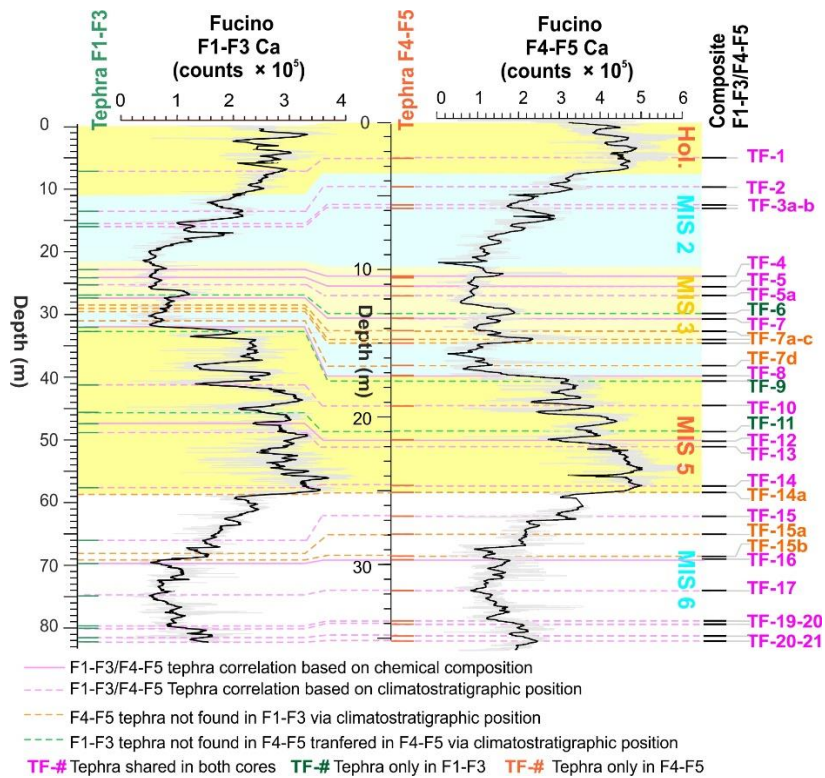


Figure 10. Detailed proxy and tephra correlation of the F1-F3 record with the corresponding interval in core F4-F5. The two tephra records are merged for a composite F1-F3/F4-F5 tephra record. Note that tephra found only in F1-F3 or F4-F5 are transferred from one to the other via climatostratigraphic positions.

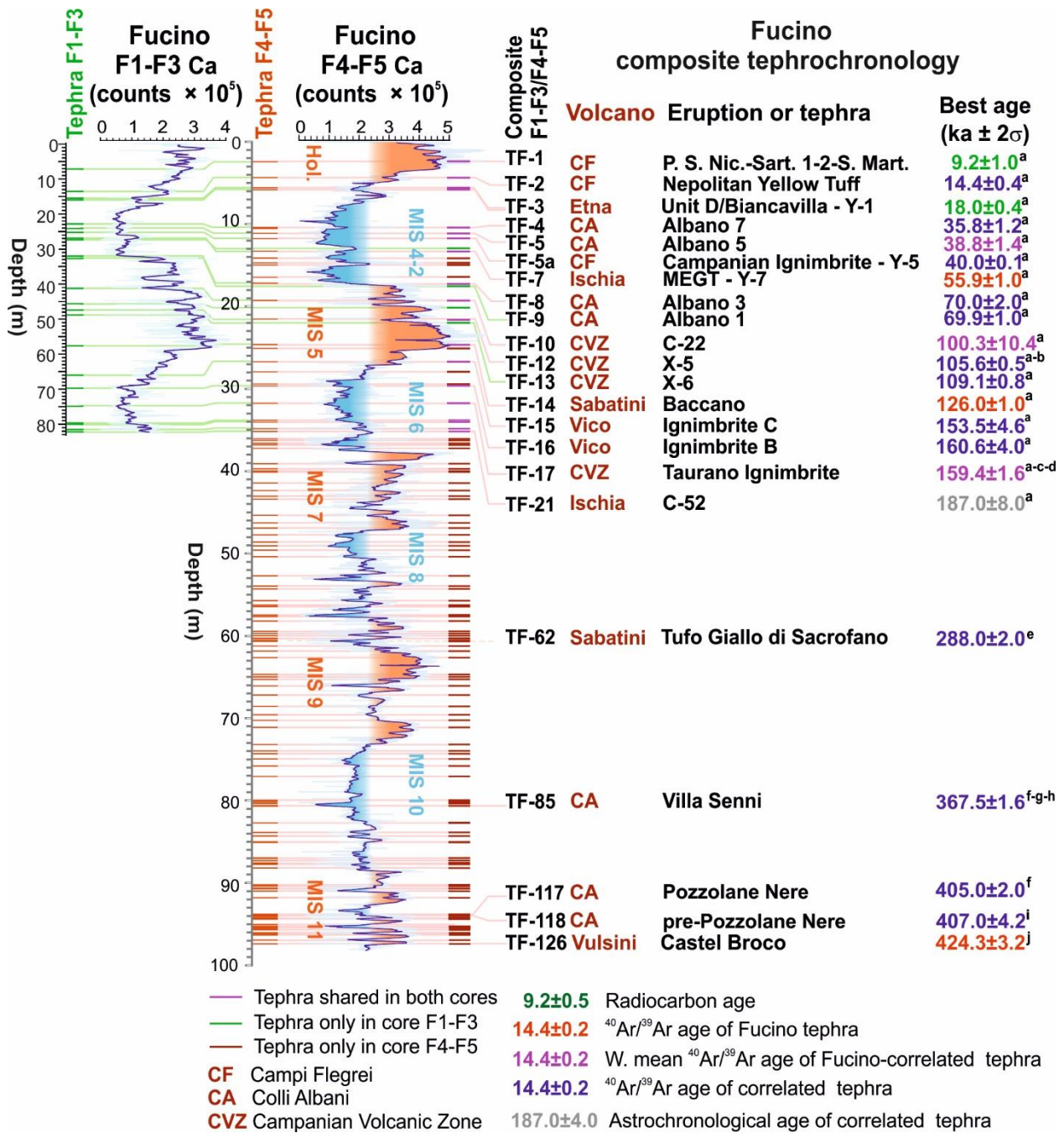


Figure 11. Composite F1-F3/F4-F5 tephra record. References: ^a Mannella et al. (2019 and references therein); ^b Petrosino et al. (2016) ^c Amato et al. (2018); ^d De Vivo et al.. (2001); ^e Sottili et al. (2010); ^f Marra et al. (2009); ^g Marra et al. (2019); ^h Giaccio et al. (2012); ⁱ Pereira et al. (2018); ^j This study. ⁴⁰Ar/³⁹Ar ages are recalculated relatively to an age of 1.1891 Ma for the Alder Creek sanidine monitor standard (Niespolo et al., 2017), with the uncertainty expressed at 2σ.

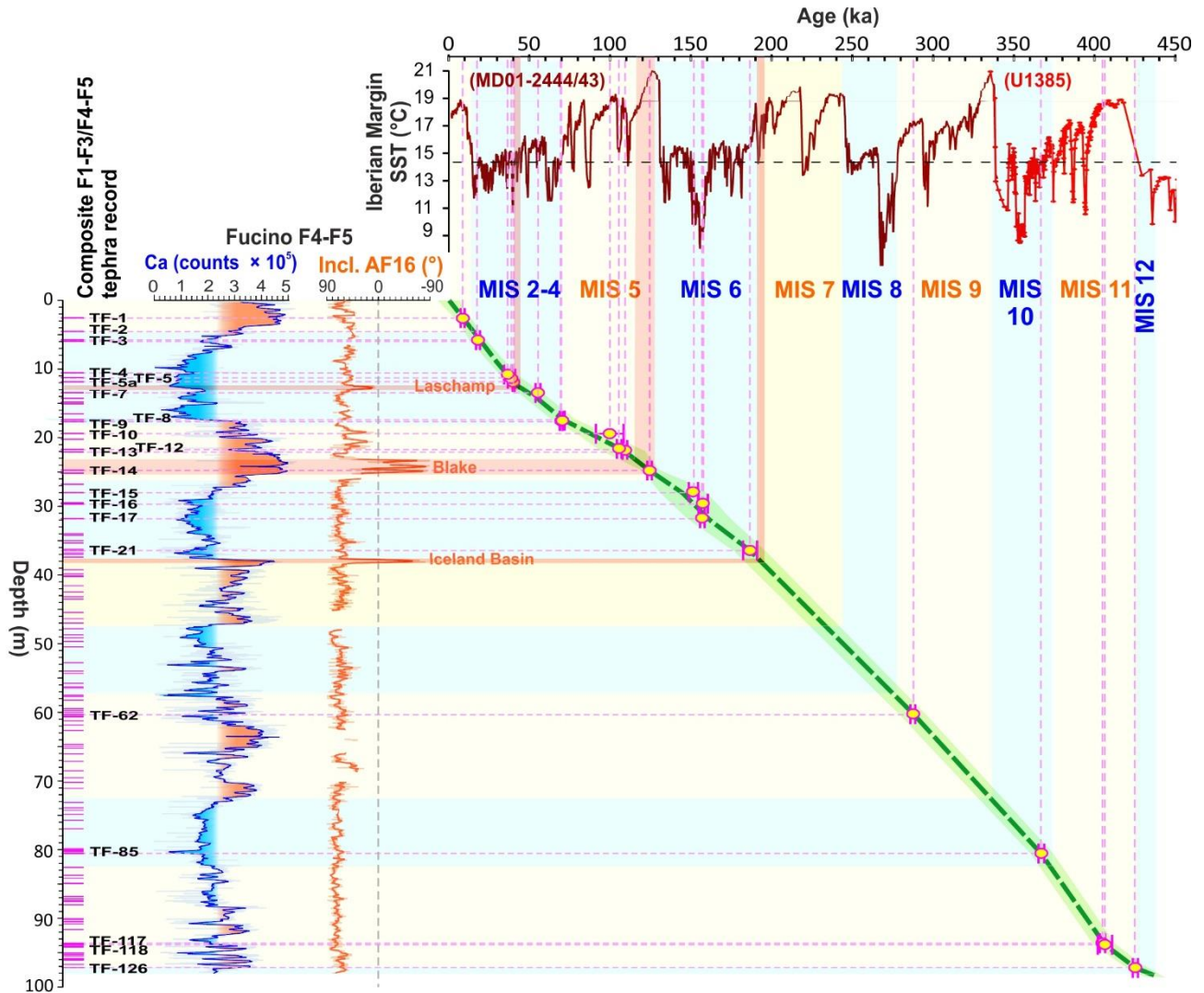


Figure 12. Preliminary age model for the composite F1-F3/F4-F5 tephra and F4-F5 Ca and palaeomagnetic records. The Fucino calcium record is compared with the sea surface temperature (SST) record from the SW Iberian Margin core MD01-2444/43 (dark red, Martrat et al., 2007) and core U1385 (red Rodrigues et al., 2017). The boundaries of the marine isotope stages (MIS) Iberian Margin record and are projected in the Fucino record along the intercept points of the yellow/blue bars with the dashed green line, which is the linear interpolation between the mid-point of the tephra ages reported in Figure 9. The ages of Fucino tephras (dashed pink lines) are in turn projected in the time-scale of the Iberian Margin SST records, that are based on their own age models (Martrat et al., 2007; Rodrigues et al., 2011). The interceptions of the orange bars with the dashed green line also provide an age estimation for the Laschamp, Blake and Iceland Basin geomagnetic excursions, as inferred from the preliminary palaeomagnetic data.

Table 1: Analysed tephra layers from core F4-F5.

Fucino tephra	Sampling code	Bottom mcd	Thickness (cm)	Main lithological features	Source
TF-4	F5-8 77-93	10.57	15.50	Darkish coarse ash made of dense blackish porphyritic scoria including crystals of leucite, pyroxene and dark mica, also occurring as abundant loose clasts. Accessory lithic made of lava and holocrystalline clasts also occur.	Colli Albani
TF-5	F5-8 148-154	11.13	~6*	Darkish coarse ash made of dense blackish porphyritic scoria including crystals of leucite, pyroxene and dark mica, also occurring as abundant loose clasts. Accessory lithic made of lava and holocrystalline clast also occur.	Colli Albani
TF-7	F5-10 147-149	14.14	2.00	Greyish medium ash made of whitish-transparent micro-pumices associated with dense brownish glass shards with abundant loose crystals of large sanidine and black mica.	Ischia
TF-8	F5-12 90-95	17.15	4.50	Darkish ash made of blackish poorly vesicular scoria associated to scarce crystals of leucite and clinopyroxene.	Colli Albani
TF-12	F5-15 90-91	21.53	1.00	Greyish to dark yellow, fine grained ash with whitish-transparent micropumices and glass shards. Stretched/elongated vesicles, only very few loose crystals of sanidine, black mica and pyroxene.	Campi Flegrei-CVZ
TF-17	F5-20 89-91	29.64	2.00	Fine to coarse grained, greyish ash with 1) greyish dark vesicular scoria; 2) brownish and transparent glass shards and micropumice; 3) coarse, (rounded) whitish and greyish pumice, with loose sanidine, clinopyroxene, and amphibole crystals	Campi Flegrei-CVZ
TF-62	F4-39 90-100	60.60	10.00	Darkish coarse ash consisting of 1) greyish dark vesicular scoria; 2) brownish and transparent glass shards and micropumice; 3) coarse, (rounded) whitish and greyish pumice, with loose sanidine, clinopyroxene, and amphibole crystals.	Sabatini
TF-85	F5-49 74-88	80.52	13.25	Darkish medium-coarse ash made of both black porphyritic leucite-bearing scoriae and aphyric highly vesicular black scoriae, along with abundant crystals of leucite and dark mica and lithics. Toward the top, the ash becomes finer.	Colli Albani
TF-117	F5-57 0-7	95.13	7.00	Darkish fine ash made of black porphyritic leucite-bearing scoriae associated with free crystals of leucite and lithics. Toward the top, the sediment evolves into a coarse ash made of blackish vesicular porphyritic scoriae along with leucite and lithics.	Colli Albani
TF-118	F5-57 16-23	95.29	7.50	Darkish fine ash made of black porphyritic scoriae along with abundant free crystals of leucite and minor lithics.	Colli Albani
TF-126	F5-58 64- 66	97.24	2.00	Light-grey medium ash made of highly vesicular white pumices associated with crystals of sanidine, plagioclase, dark mica and opaques and glass shards and minor lithics. Toward the top, the sediment turns to a dark grey-blackish medium ash.	Vulsini

*Base of tephra inside of the core-catcher, not in composite depth.

Supplementary materials

SD1: Full data set of the tephra glass major element composition (WDS-EMPA).

SD2: Full data set of the $^{40}\text{Ar}/^{39}\text{Ar}$ dating.

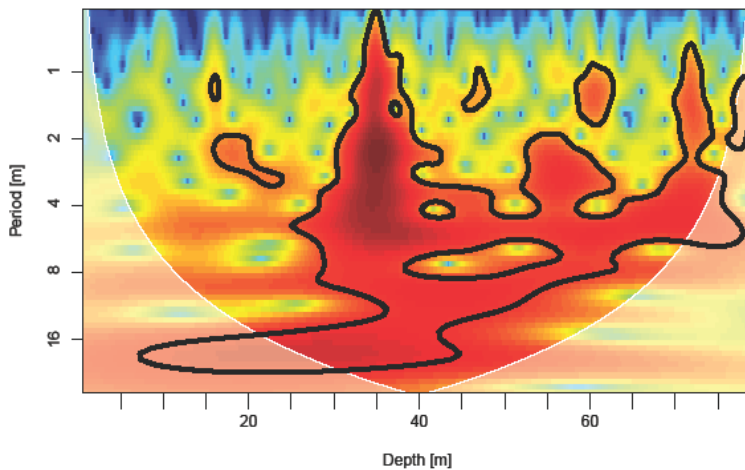


Figure S1. Wavelet analysis of the gamma ray dataset from F4 borehole. The white shading indicates areas outside the cone of influence that should be taken with care. Red colours indicate strong cyclic behaviour, and blue colours no cyclic behaviour of the data. The bold line represents the results of a significance test, for details see Gouhier et al. (2018) and the appended R script.